THE ASTROPHYSICAL JOURNAL, 407:806–819, 1993 April 20

DUST COAGULATION

ARATI CHOKSHI
IPAC/Caltech, Pasadena, CA 91125
AND
A. G. G. M. TIELENS AND D. HOLLENBACH
NASA-Ames Research Center, Moffett Field, CA 94035
Received 1992 February 5; accepted 1992 October 23

ABSTRACT

Two colliding dust particles can stick, bounce, fragment, melt, or vaporize upon collision, depending on the relative velocity and material parameters. We have theoretically modeled the microphysics of the coagulation process in the collision of two, smooth, elastic, spherical grains. It is shown that sticking will occur when the relative collision velocity is less than a critical velocity, v_{cr}, which depends on the grain size and the elastic properties and surface energy of the material. Critical relative velocities for coagulation have been evaluated as a function of grain sizes for silicate, icy, and carbonaceous grains. We find that v_{cr} varies as $R^{-5/6}$ where R is the radius of curvature of the colliding particles. Micron-sized quartz particles are able to coagulate at collision velocities of less than $\simeq 10^2$ cm s^{-1}, while centimeter-sized grains require velocities below 10^{-2} cm s^{-1}. Critical velocities also depend on the material properties (interface energy and elasticity) of the particles; thus small icy grains stick better than small quartz grains (v_{cr} is $\simeq 2 \times 10^3$ cm s^{-1} vs. 10^2 cm s^{-1} for 1000 Å grains).

Realistic interstellar grains may be nonspherical and have core mantle structure and rough surfaces. In addition, plastic flow may also be of importance. The role of these effects in the coagulation process is examined. It is concluded that nonsphericity has only a minor effect. Surface irregularities can limit coagulation considerably. For submicron-sized ice grains this may reduce the critical velocity by a factor $\simeq 3$. For silicate and graphite grains this reduction may be much larger. While plastic deformation is very important in the collision of centimeter-sized metal spheres, micron-sized grains have a much higher yield strength, and their sticking will not be affected much. Finally, we briefly examine sticking in the collision of fluffy agglomerates.

Coagulation of interstellar grains in dense clouds is briefly discussed. We conclude that efficient coagulation requires coverage of grain cores by an icy grain mantle. Even then, coagulation will lead to only a doubling of the mass of a large ($a > 1000$ Å) grain within a dense core lifetime. Smaller grains can, however, be efficiently removed from the cloud by coagulation. Thus, coagulation can have a dramatic effect on the visible and, particularly, the UV portion of the extinction curve in dense clouds and on their IR spectrum.

Subject headings: dust, extinction — interstellar: grains — interstellar: matter — planets: formation

1. INTRODUCTION

Dust is associated with diffuse and dense interstellar medium, permeates the solar interplanetary medium, and is observed in envelopes and disks around stars and planets. In the diffuse interstellar medium the grain sizes are observed to range from typical molecular sizes (~ 5 Å) to about 2500 Å (see Mathis, Rumpl, & Nordsieck 1977; Mathis 1990; Tielens 1990a). Some of this dust originates in the outflows from red giants (Merrill 1977). Besides nucleation and chemical growth, coagulation plays an important role in the grain growth process in this environment (Tielens 1990b). Likewise, coagulation is thought to be important for grain growth in the interstellar medium. In particular, visible extinction and polarization measurements toward objects embedded in or behind dense clouds indicate the presence of larger grains than in the diffuse ISM (Whittet & van Breda 1978). There are two mechanisms which can perpetuate grain growth in these dense environments: (1) accretion of gas phase atoms and molecules on preexisting grains forming icy grain mantles, and (2) coagulation of colliding smaller grains. Indeed, IR absorption studies indicate the presence of icy mantles around grains in these kinds of environments (see Tielens 1989). However, most of this ice will be on the smallest grains, and ice mantle formation by itself will not lead to a substantial increase (≤ 175 Å) in the grain size of the large grains (~ 1000 Å) responsible for the visible extinction (Draine 1985). Coagulation is therefore a viable and an attractive alternative for appreciable grain growth in dense molecular clouds and in circumstellar outflows.

Coagulation has also played an important role in the formation of the solar system. The planetesimals that went into forming the planets must have formed from smaller bodies such as surviving interstellar grains and condensates from the gas of the solar nebula. These small grains grew by coagulation until they were big enough to decouple from the gas and settle in a dusty disk. Further coagulation in this disk leads then to the formation of planetesimals and eventually planets (Weidenschilling & Cuzzi 1993). Direct observational evidence for the importance of coagulation in the solar nebula has been preserved in interplanetary dust particles collected in Earth's upper atmosphere. These particles are aggregates of smaller particles with sizes of ~ 1000 Å and are likely largely unmodified remnants of the planetary formation processes (Brownlee 1987; Bradley, Sandford, & Walker 1988).

In spite of the recognized importance of the coagulation phenomenon, the physics of the process itself has been poorly

studied in an astrophysical context. Studies of grain-grain collisions (Weidenschilling 1980, 1984; Volk et al. 1980; Scalo 1977) have generally focused on the evolution in the dust size distribution due to collisions involving specific size distributions and velocity fields. In some cases, the coagulation criterium used is based upon an adhesion theory (Dahneke 1972) which is known to be incorrect (Derjaguin, Muller, & Toporov 1975). In other studies, the consequences of coagulation of dust grains are determined using sticking probabilities of either zero or unity depending on whether the particle collisions occur at energies greater or less than the attractive potential between particles. Although intuitively plausible, this assumed value for the critical velocity has no firm theoretical basis. Here we focus on the coagulation process itself and the derivation of critical velocity with its dependence on size and material properties of the colliding particles.

Stickiness of materials has been better explored in fields of aerosol science, colloidal physics, and material surface and interface science (Zebel 1966; Kendall 1980). Aerosol particles collected in the atmosphere or soot particles formed in laboratory experiments consist of a large number of small (100–1000 Å) spherical grains arranged in a very porous and fluffy network. Figure 1 shows an example of such a collisional agglomorate observed in a high-resolution transmission electron microscope study of the condensation of silicon vapor (Iijima 1987). As Figure 1 illustrates, when two particles come together, they are compressed at their contact point and form a finite contact area. The earliest observations of contact areas between surfaces were by Newton in his famous Newton's Rings experiment. He deduced that two convex surfaces made perfect contact at their contact point from the observation of the "black spot" at the center of the reflected rings. Classical work in the study of contacts between spherical and ellipsoidal surfaces was done by Hertz (1896) who derived an empirical expression for the size of the contact area as a function of the applied force. In more recent years, laboratory experiments have shown that even in the absence of an external force, two spherical particles meet at a finite contact circle due to the mutual attraction of the particles, and a pull-off force is required to separate the equilibrium contact between two particles (Johnson, Kendall, & Roberts 1971; Kendall 1980). This force, which can be due to either van der Waals or chemical interaction, drives coagulation.

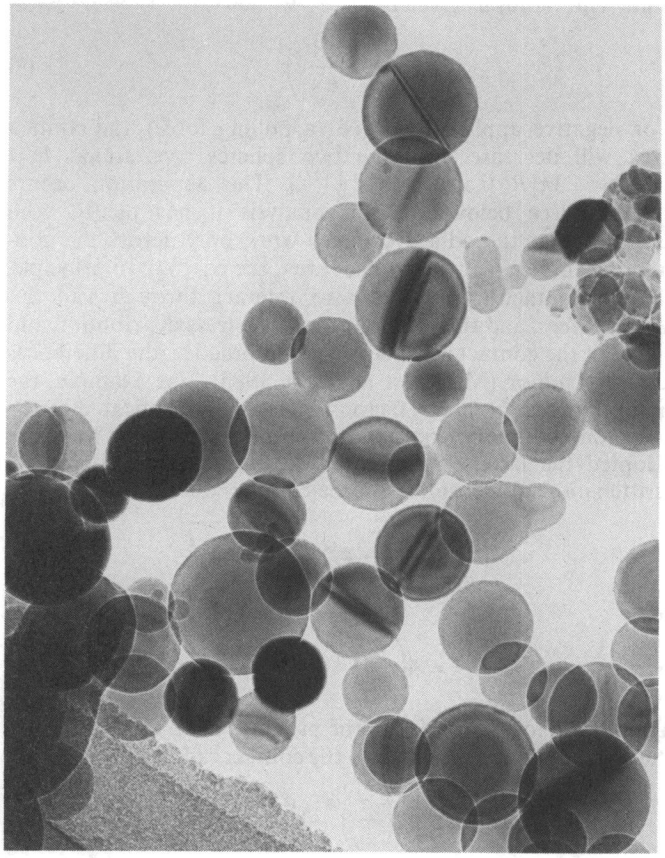

FIG. 1.—Electromicrograph showing coagulated spherical Si particles, prepared by a gas evaporation method (Iijima 1987). The dark bands are caused by planar faults. Note the neck formed by the two grains touching on the mid-right. A typical grain has a diameter of 700 Å.

In this paper we explore the microphysics of coagulation between two, colliding, smooth, spherical grains in the elastic limit and calculate the criteria for sticking as a function of particle sizes, collision velocities, elastic properties, and binding energy. In § 2 we present a theoretical description of the coagulation process and derive the sticking criteria. The critical collision velocity, below which two spheres will stick, is derived for silicate, carbon, and icy spheres in this section as well. The effects of nonsphericity, rough surfaces, core-mantle structures, and plastic deformation are discussed in § 3. Sticking in the collision of fluffy conglomerates of particles is also briefly discussed in this section. The results are applied to coagulation in dense interstellar clouds in § 4. Conclusions are presented in § 5.

2. COAGULATION OF COLLIDING GRAINS

We study the process of grain-grain collisions from a macroscopic point of view using elastic continuum theory for the description of solids. Grains are treated as spherical, smooth particles that experience only elastic deformation when subjected to a load. For astrophysically relevant conditions, particle sizes ~ 50 Å to $\sim$few μs and velocities ~ 10 cm s^{-1} to ~ 0.1 km s^{-1}, plastic deformation is unimportant (see §§ 2.5 and 3.4). For fluffy collisional aggregates, other energy loss channels, besides elastic and plastic deformation, open up (i.e., crushing; § 3.5).

When two spherical grains approach one another they first experience a long-range attraction primarily caused by the van der Waals interaction. The particles accelerate in the attractive potential and collide with a collision energy which is the sum of the initial relative kinetic energy and the attractive energy. Upon contact, the collision and attractive energies excite elastic waves, and, near the contact point, these will constructively interfere and the grain will elastically deform, resulting in a flattened contact area. The attractive forces across the contact area form the incentive to coagulate. The two grains come to rest when the initial kinetic energy and the attractive interaction energy balances the repulsive elastic energy. This stored elastic energy will tend to spring the two grains apart, but some of the elastic energy will remain behind as internal elastic wave excitation. Sound wave dissipation time scales are long compared to the collision time scales of micron-sized dust grains (see § 2.2.4). Nevertheless, sticking will still occur if, after the collision, the internal elastic wave energy is larger than the initial kinetic energy. The two grains are then left vibrating in their interaction potential well until eventually all the interaction energy is dissipated by the damping of the elastic waves. We can define a critical velocity, v_{cr}, at which the kinetic energy

at infinity is equal to the elastic wave energy left behind in the grains just after the collision. Thus, for collision velocities below v_{cr}, sticking will occur, while above v_{cr} the grains will just bounce.

In the remainder of this section, we will examine the interaction of two colliding grains, using a quasi-static treatment (§ 2.1). This will lead to a simple expression for the excitation energy left behind at the end of the collision. Then, following Rayleigh (1906), we will probe the accuracy of this quasi-static treatment (§ 2.2). This will result in an improved sticking criterium (§ 2.3) we will compare our theoretical results with those of Rayleigh for nonsticky solids and in § 2.5 with experiments.

2.1. *The Quasi-static Approach*

In the quasi-static treatment, we will assume that the deformation of the colliding bodies is restricted to the contact zone and its shape and magnitude are given by static elastic theory: that is, the deformation is governed by the instantaneous force between the two bodies and not by its history. This is equivalent to assuming that elastic wave motion in the bodies can be ignored. Thus, we visualize it as a collision (at low velocities) between two cars (Johnson 1989). The bumpers, connected by springs to the main framework, take the brunt of the collision (i.e., deform), while the cars themselves are slowly decelerated without deformation. The validity of these assumptions will be assessed in § 2.2.

Ignoring the attractive interaction, two spheres of radii R_1 and R_2 in contact under an impressed static force F will maintain an equilibrium contact circle with a radius a given by (Hertz 1896; Landau & Lifshitz 1959)

$$a = (3RF/4E)^{1/3} . \tag{1}$$

Here $R = R_1R_2/(R_1 + R_2)$ is the "reduced" radius of the particles and $1/E = [(1 - \nu_1)^2/E_1 + (1 - \nu_2)^2/E_2]$, with ν_i and E_i Poisson's ratio and Young's modulus of grain i. For a much less than R, the elastic displacement, δ, along the lines connecting the two spheres is the sum of the displacement δ_i of each sphere (see Fig. 2). The latter is given by

$$\delta_i = a^2/R_i . \tag{2}$$

The elastic deformation energy associated with such a contact area can be calculated from

$$U_E = \int F\, d\delta \tag{3}$$

or

$$U_E = 8Ea^5/15R^2 . \tag{4}$$

Consider now the case with attractive surface energy. The binding energy at the contact circle is

$$U_S = -2\pi a^2\gamma , \tag{5}$$

where γ is the surface energy per unit area of each surface. For two dissimilar surfaces, the surface energy is equal to $\gamma_1 + \gamma_2 - 2\gamma_{12}$ where γ_1 and γ_2 are the intrinsic surface energies of the two solids and γ_{12} is the interface energy. For van der Waals interaction, the combining law, $\gamma = \sqrt{(\gamma_1 \times \gamma_2)}$, is often used. Although this is known to give an upper limit, the error is often not larger than a few percent (Israelachvili & Tabor 1973). With an attractive surface energy, a force is required to separate the two spheres even in the absence of an external force. Theoretical and experimental studies of static adhesion between spheres have shown that this force is given by $F = -F_c$ where

$$F_c = 3\pi\gamma R \tag{6}$$

(Johnson et al. 1971; Kendall 1980; Muller, Yushchenko, & Derjaguin 1980, 1983). Note that this pull-off force is independent of the elastic properties of the grains making contact. In the presence of attractive surface energy, the stress distribution at the contact surface between two spheres is modified from the Hertzian equilibrium solution. Evaluation of this stress distribution leads to the following modification of the equation describing the forces between the spheres (Johnson et al. 1971)

$$F = \frac{4Ea^3}{3R} - 2\pi a^2\sqrt{\frac{4\gamma E}{\pi a}} , \tag{7}$$

where the first term is the Hertzian relation between force and contact radius in the absence of adhesion (eq. [1]). Solving for the contact radius, we find

$$a = \left\{\left(\frac{3R}{4E}\right)[F + 6\pi\gamma R \pm \sqrt{(6\pi\gamma R)^2 + 12\pi\gamma RF}]\right\}^{1/3} , \tag{8}$$

where only the positive root is allowed for stable equilibrium (i.e., $F \geq -F_c$). Thus, when two spheres are brought into contact under a force F, the contact area will be larger than in the Hertzian case due to the attractive interaction. Furthermore, at zero external force, the equilibrium contact area is finite with radius a_0 given by

$$a_0 = \left(\frac{9\pi\gamma R^2}{E}\right)^{1/3} . \tag{9}$$

For negative applied force (i.e., a pulling force), the contact area will decrease until the two spheres separate at $F = -F_c = -3\pi\gamma R$ (i.e., $a/a_0 = [\frac{1}{6}]^{2/3}$). This separation occurs abruptly (see below). In this analysis it has tacitly been assumed that the adhesive forces work only across the contracting surface (i.e., the contact area; see eq. [5]). In principle, the noncontacting surfaces also interact through van der Waals forces, and this will influence the stress distribution and shape of the contact area. However, in practice, the differences are very minor (Muller et al. 1980, 1983). For example, the pull-off force is at most a factor 4/3 larger than indicated by the pure contact theory (eq. [5]). For simplicity, we have therefore adopted the latter. Using equation (9), equation (8) can be written into a dimensionless force-contact radius relation

$$4\left(\frac{a}{a_0}\right)^3 = \frac{F}{F_c} + 2 + 2\sqrt{1 + \frac{F}{F_c}} \tag{10}$$

or

$$\frac{F}{F_c} = 4\left(\frac{a}{a_0}\right)^3 - 4\left(\frac{a}{a_0}\right)^{3/2} , \tag{11}$$

again, valid for $F \geq -F_c$. In the presence of an adhesive force, the displacement δ is related to the contact radius by

$$\frac{\delta}{\delta_c} = 6^{1/3}\left[2\left(\frac{a}{a_0}\right)^2 - \frac{4}{3}\left(\frac{a}{a_0}\right)^{1/2}\right] , \tag{12}$$

where

$$\delta_c = \frac{1}{2}\frac{a_0^2}{(6^{1/3}R)} . \tag{13}$$

Under a tensile (separating) force, the spheres stretch, form a neck connecting the two, and finally separate at the critical displacement $\delta = -\delta_c$ (see Fig. 2 and below).

The surface energy and elastic deformation energy in dimensionless units are now

$$\frac{U_S}{F_c \delta_c} = -\frac{4}{3} 6^{1/3} \left(\frac{a}{a_0}\right)^2 \quad (14)$$

and

$$\frac{U_E}{F_c \delta_c} = 2 \times 6^{1/3} \left[\frac{8}{5}\left(\frac{a}{a_0}\right)^5 - \frac{8}{3}\left(\frac{a}{a_0}\right)^{7/2} + \frac{4}{3}\left(\frac{a}{a_0}\right)^2\right]. \quad (15)$$

The total potential energy (U_r) in the collision process is the sum of the attractive surface binding energy and the repulsive elastic energy of deformation ($U_S + U_E$),

$$\frac{U_T}{F_c \delta_c} = 2 \times 6^{1/3} \left[\frac{8}{5}\left(\frac{a}{a_0}\right)^5 - \frac{8}{3}\left(\frac{a}{a_0}\right)^{7/2} + \frac{2}{3}\left(\frac{a}{a_0}\right)^2\right]. \quad (16)$$

The collision process is schematically illustrated in Figure 2, and the solutions to the dimensionless equations (11), (12), (14), (15), and (16) that govern the collision are shown in Figure 3. Some dimensionless values for the parameters in the collision process are collected in Table 1. We have also evaluated the characteristic scale lengths, a_0 and δ_c, the characteristic force, F_c, and the characteristic energy, $F_c \delta_c$, for two 1000 Å grains of various materials in Table 2. The material parameters employed are listed in Table 3. To calculate the interface energy of water ice, we used a bond energy of 0.5 eV/bond and a bond length of 3.1 Å, which is typical for hydrogen bonding in ice. This hydrogen bond interaction is stronger than the van der Waals attraction between water molecules and will dominate the interface energy for icy surfaces. For silicate particles we have adopted the experimental value for γ measured from contact area of submicron quartz particles (Kendall, Alford, & Birchall 1987). This is the typical value for van der Waals interaction. Much larger values are expected for chemical bonding of oxide surfaces (300 and 1000 ergs cm^{-2} for amorphous and crystalline surfaces, respectively; van Vlack 1965). However, since accretion and diffusion time scales for gas atoms onto grain surfaces are short, any dangling chemical bonds will be rapidly saturated (Tielens & Allamandola 1987). Thus, we expect that this larger theoretical value will not be attained. An interface energy of about 3000 ergs cm^{-2} has been determined from electron microscopy studies of the contact area of submicron Fe-Ni grains (Easterling & Thölen 1972). This difference in interface energy between small oxide and metallic grains merely reflects the difference between a largely covalent and metallic bond. The value for the graphic surface quoted in Table 2 is that for the basal plane. Again, it is likely that any dangling chemical bonds in the aromatic planes will be rapidly saturated with H in the interstellar space.

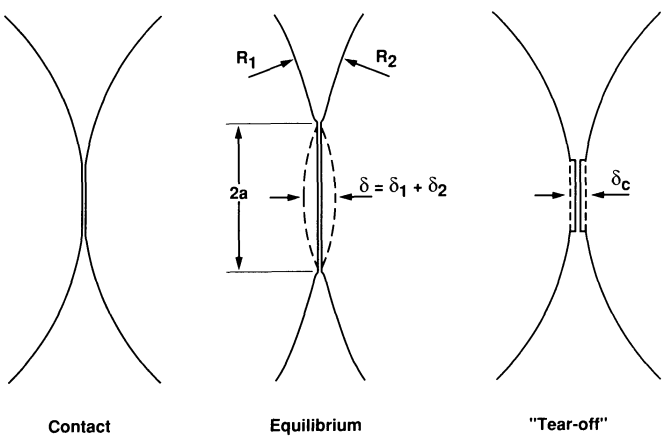

FIG. 2.—Schematic of the deformation during the collision process. At contact, a finite contact area is rapidly formed. This contact area grows in size during the compression and slowing down of the collision partners. Upon reversal of the collision process, the two grains will pull out a neck area, until they separate at a critical displacement, δ_c. See text for details.

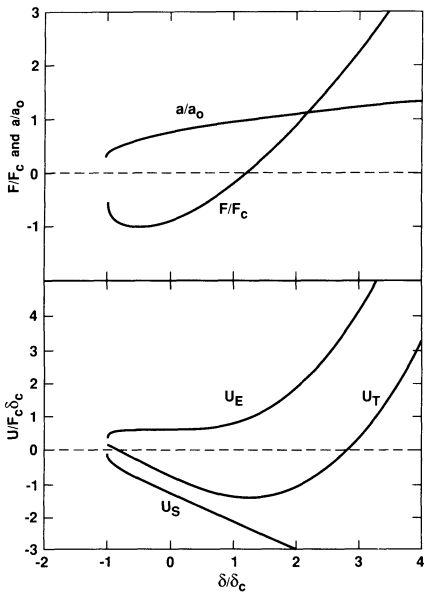

FIG. 3.—Size of the contact area, a, the force, F, the surface energy, U_S, elastic energy, U_E, and total energy, U_T, are shown in dimensionless form. Here a_0 is the equilibrium contact size, F_c is the critical force required to separate the two grains, and δ_c is the critical displacement (*see text*).

TABLE 1

CHARACTERISTICS OF THE COLLISION PROCESS

Parameter	δ/δ_c	a/a_0	F/F_c	$U_T/F_c\delta_c$
Contact	0	$(2/3)^{2/3}$	−8/9	$-(8 \times 4^{2/3}/15)$
Equilibrium	$(4/3)^{2/3}$	1	0	$-(4 \times 6^{1/3})/5$
δ_{max}[a]	2.79	1.23	1.96	0
Tear-off.....	−1	$(1/6)^{2/3}$	−5/9	4/45

[a] Maximum compression, calculated assuming no initial velocity upon contact.

TABLE 2

TYPICAL COLLISIONAL PARAMETERS[a]

Material	a_0 (Å)	δ_c (Å)	F_c (dyn)	$F_c\delta_c$ (eV)
Quartz.....	20	0.3	2.4 (−3)	4.5
Polystyrene	40	1.1	1.1 (−3)	7.6
Graphite	50	1.7	7.1 (−3)	75
Iron.....	65	2.9	2.8 (−1)	5100
Ice	100	6.9	3.5 (−2)	1500

[a] Evaluated for the collision of two equal 1000 Å grains.

TABLE 3

MATERIAL PARAMETERS

Material	γ^a (ergs cm^{-2})	E (dyn cm^{-2})	ν	ρ (g cm^{-3})	Reference
Quartz	25[b]	5.4 (11)	0.17	2.6	1, 2
Polystyrene	12	3.4 (10)	0.5	1.04	2, 3
Graphite	75	1.0 (11)	0.32	2.2	4, 5
Iron	3000	2.1 (12)	0.27	7.7	2, 6
Ice	370[c]	7.0 (10)	0.25	1.0	7

[a] Surface energy per surface.
[b] Measured for micron-sized particles (see text).
[c] Estimated from the H-bonding energy and a bond length of 3 Å.
REFERENCES: (1) Kendall et al. 1987; (2) Physics Vademecum; (3) Kendall & Padget 1987; (4) Brocklehurst 1977; (5) Zisman 1963; (6) Easterling & Thölen 1972; (7) Gaffney 1985.

The characteristic length scales, a_0 and δ_c, in Table 2 have been evaluated for the collision of two equal 1000 Å grains. The calculated values range from 20 to 100 Å for a_0 and 0.3 to 7 Å for δ_c. Comparing the values for the different materials, we note that ice grains have an about 5 times larger a_0 than quartz due to the larger surface energy (i.e., larger attractive force) and the lower Young's modulus (i.e., more readily deformed). As a result, we expect ice grains to stick much better.

The collision process can be schematically summarized as follows. Recalling our earlier discussion, upon contact ($\delta/\delta_c = 0$) the two colliding grains rapidly form a finite contact area under influence of the attractive forces. This is essentially the inverse of the opening of a "Griffith" crack (Kendall 1980) and occurs on the sound travel time scale; much faster than the collision time scale (see below). The released excess energy (i.e., $|U_S - U_E|$) will initially accelerate the two grains and δ/δ_c will increase. The two grains will pass the equilibrium separation (i.e., $F/F_c = 0$; see Table 1) and then will be decelerated by the compression until they are brought to a halt. At that point, the stored elastic energy of deformation will reverse the collision process, and δ/δ_c will decrease. When the two grains reach the point $\delta/\delta_c = 0$ again, the contact area is finite, and the total energy is negative. Thus, the two grains are still bound by the attractive forces across the contact area. Now, although δ will be negative from here on, the two grains are still connected by a neck and bound across the contact area. Finally, at the point $\delta = -\delta_c$, the contact between the two spheres becomes unstable (i.e., $\partial F/\partial a \rightarrow \infty$), and the contact will rupture, again similar to the opening of a "Griffith" crack. The energy required to break the surface bonds when a decreases is exactly provided by the released elastic energy of deformation (i.e., $\partial U_S/\partial a|_\delta = \partial U_E/\partial a|_\delta$). However, the total energy U_T is positive at this point (i.e., $U_E > U_S$). Just prior to snapping, the two spheres will still be pulled out in a cone-type structure with a height δ_c. The elastic deformation energy associated with this "cone-type" deformation will remain behind after the two grains separate. From equation (16) we calculate this to be $12/135 F_c \delta_c$ (Table 1). Thus, from this first-order calculation, we conclude that, if the initial kinetic energy of the two colliding grains is larger than $\simeq 0.09 \times F_c \delta_c$, they will be able to separate. Otherwise they are trapped in their potential well and remain bound. This is a strict lower limit to the initial kinetic energy required to separate, since we assumed that deformation was confined to the contact area (i.e., quasi-static approach). In reality, a large amount of elastic energy may go into deforming the two grains outside the contact area. We will estimate this in the next section.

2.2. *Deformation of the Colliding Grains*

In the previous section, a quasi-static analysis of the collision process led us to conclude that a small fraction of the interaction energy stays behind after separation due to the deformation near the contact area. Following Rayleigh (1906), we will now make a second-order approximation to the energy in elastic waves remaining in the grains after the collision, taking the deformation of the whole grain into account. The forces acting between the two grains will be approximated by the quasi-static result derived in the previous section (eq. [11]). The energy in the spheres after the collision can then be calculated from a Fourier analysis of this forcing function. We will now first develop the forcing function in time-dependent form. Second, we will discuss the vibrational modes of a solid sphere. Finally, we will determine the excitation of these modes during the collision process. This analysis will yield the energy in these modes staying behind after the collision.

2.2.1. *The Collision Time Scale*

Consider again two spheres of masses m_1 and m_2 approaching one another with relative velocity v_∞ at infinity. The spheres are first accelerated by the long-range van der Waals attraction, given by $F = AR/6z^2$ with A the Hamaker's constant of the two materials and z the separation between the two spheres (Tabor 1977; Israelachvili & Tabor 1973). The collision energy $U_{\rm col}$, is then

$$U_{\rm col} = \tfrac{1}{2}\mu v_{\rm col}^2 = \tfrac{1}{2}\mu v_\infty^2 + 2\pi R \gamma_0 z_0 , \qquad (17)$$

where $v_{\rm col}$ is the velocity at the instant of contact. The second term on the right-hand-side describes the van der Waals interaction, with γ_0 the surface energy per unit area due to van der Waals interaction ($\gamma_0 = A/[24\pi z_0^2]$, with A Hamaker's constant). The distance of first contact, z_0, is the equilibrium distance in the van der Waals potential of two atoms making contact. Typically, z_0 is about 4 Å. Since this van der Waals acceleration is independent of the deformation process, we can add this term to the initial kinetic energy of the collision.

The energy equation of the system can be written as

$$U_{\rm col} = U_E + U_S + \tfrac{1}{2}\mu\dot{\delta}^2 = U_T + \tfrac{1}{2}\mu\dot{\delta}^2 , \qquad (18)$$

where μ is the reduced mass of the colliding particles $\mu = m_1 m_2/(m_1 + m_2)$. The three terms on the right-hand side are, respectively, the energy of deformation, the attractive interaction energy, and the instantaneous energy of motion. In the computation of the collision time, it is advantageous to divide the collision into the incoming (δ increasing) and outgoing

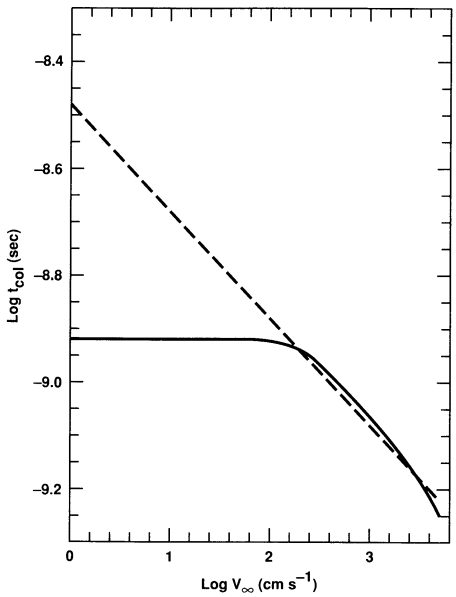

FIG. 4.—Collision time scale, t_{col}, as a function of the initial velocity, v_∞ for the collision of two 1000 Å graphite spheres (*solid line*). The Hetzian solution (*dashed line*) is also shown.

(δ decreasing) parts. The collision time can now be determined from

$$t_{col} = \int_0^{t_{col}} dt = \int_{\delta=0}^{\delta=\delta_{max}} \frac{d\delta}{v} + \int_{\delta=\delta_{max}}^{\delta=-\delta_c} \frac{d\delta}{v}, \qquad (19)$$

where δ_{max} is the maximum displacement (i.e., $v[\delta_{max}] = 0$). We also define t_{max} as the time scale to reach maximum compression (i.e., $\delta = \delta_{max}$), which can be similarly calculated.

We have evaluated the collision time scale from equation (19) numerically for two equal 1000 Å graphite grains colliding at various velocities. These are compared to Rayleigh's results for collisions without adhesion ($t_{col} \simeq 5[C_s/v_\infty]^{0.2}[R/C_s]$ s; Rayleigh 1906) in Figure 4. For low collision velocities, the collision time scale calculated including adhesion approaches a constant value determined by the deformation induced by the attractive potential. The collision time scale is then much larger than derived by Rayleigh (1906). For high collision velocities, our results asymptote to Rayleigh's results. From Figure 4, we see that the collision time scale is typically 10^{-9} s for low collision velocities.

2.2.2. *Elastic Waves*

The elastic vibrations of a solid sphere have been discussed in detail by Love (1944). Assuming azimuthal symmetry around the contact point, the angular dependence of the modes of vibration is given by Legendre functions of order n (Thölen 1980). This is illustrated schematically in Figure 5. The angular frequency of the waves is given by

$$\omega_n = \frac{2\pi c}{\lambda_n},$$

where c is the wave velocity which is approximately equal to the velocity of sound in the material ($c_s \simeq 0.93\sqrt{E/\rho}$) and λ_n is the wavelength of the nth excited mode, which is given by

$$\lambda_n = \frac{2\pi R}{\sqrt{n(n+1)}}, \qquad (20)$$

with R the radius of the sphere.

In order to make a flattened contact area of size a, elastic waves of order $\tilde{n}$ have to be appreciably excited, where

$$\tilde{n} \simeq R/a. \qquad (21)$$

Thus, for a 1000 Å graphite grain with a surface energy of 75 ergs cm^{-2}, a is approximately 50 Å (Table 2) and $\tilde{n}$ is thus ~ 20. For centimeter-sized particles, a is ~ 10 μm, and $\tilde{n}$ is ~ 1000. For a 1000 Å grain with $c_s \simeq 2 \times 10^5$ cm s^{-1}, the frequency of the lowest mode is approximately 2×10^{10} s^{-1}, and, for all relevant collision velocities, the collision time scale ($t_{col} > 10^{-9}$ s) is much longer than the period of even the lowest mode. As a result many modes will couple equally well

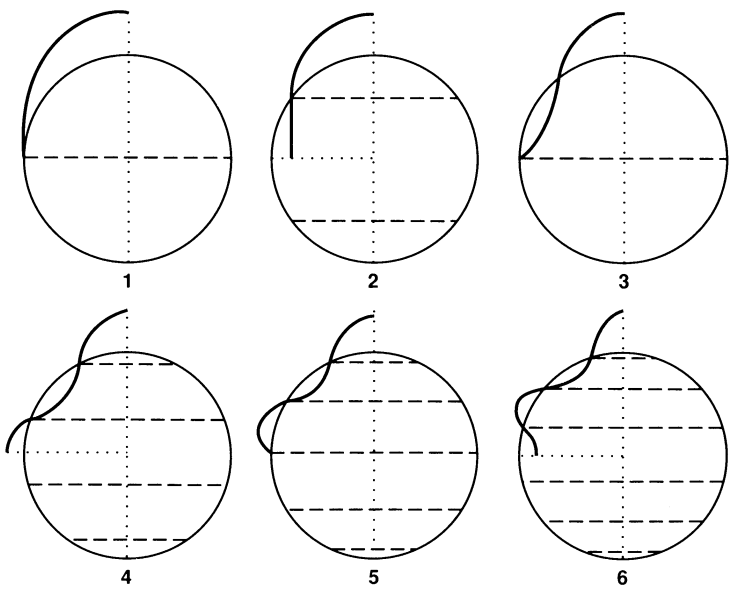

FIG. 5.—Schematic of the deformation associated with the lowest elastic vibrations of a sphere

to the forcing function. Moreover, since the collision time is so much larger than the sound travel time across the contact area ($\simeq 3 \times 10^{-12}$ s for a 1000 Å grain), the elastic state of the two bodies near the point of impact will be nearly the same as that produced by the (instantaneous) force, assuming it to be in equilibrium. This justifies our quasi-static approach in deriving the forcing function and the deformation near the contact area (Hertz 1896; Rayleigh 1906; Johnson 1989).

Following Rayleigh's treatment (1906) the equation of motion for mode n may be written as

$$\ddot{\phi}_n + \omega_n^2 \phi_n = F/a_n , \tag{22}$$

where ϕ_n is the displacement due to the nth vibrational mode, F is the forcing function (see eq. [11]), and a_n is the coefficient of inertia associated with this mode. For the lowest mode, a_1 is of the order of the mass of the sphere. For higher modes, a_n is a decreasing function of the mode number. Equation (22) has a solution given by a simple convolution equation of the form (Rayleigh 1906)

$$a_n \phi_n(t) = \frac{1}{\omega_n} \int_0^t \sin\,[\omega_n(t - t')] F(t') dt' . \tag{23}$$

For a collision that occurs between 0 and t_{col}, the wave excitation for any time $t \geq t_{col}$ is given by

$$a_n \phi_n(t) = \frac{1}{\omega_n} \int_0^{t_{col}} \sin\,[\omega_n(t - t')] F(t') dt' . \tag{24}$$

Using the forcing function, $F(\delta)$ and the compression, $\delta(t)$, given by the (numerical) solution of equations (11) and (19), $a_n \phi_n$ can be evaluated from equation (24). Figure 6 shows the results for two modes, $n = 1$ and 10, at three different collision velocities of two 1000 Å grains: (1) $v_{col} = 0$, (2) $v_{col} \sim v_{cr}$, the critical velocity for sticking, and (3) $v_{col} \gg v_{cr}$. During the collision, the convolution of a sinusoidal wave with the forcing function will generate beats with frequencies $\omega_n + \omega_c$ and $\omega_n - \omega_c$, where ω_c is the frequency associated with collision. These can be readily recognized in Figure 6. When $\omega_n t_{col} \gg 1$ (i.e., $n = 10$ in Fig. 6), the envelope defined by these beats essentially delineates the shape of the forcing function (in time coordinates). We note that, when the initial collision velocity is low, the forcing function is quite asymmetric in time. This hysteresis merely reflects the importance of adhesion in such cases (see Fig. 3). For high initial velocities, the symmetric forcing function (in time) of the Hertzian case (i.e., no adhesion) is recovered.

In the calculations reported in Figure 6, it has been assumed that at $t = t_{col}$ the collision is over and the forcing function no longer operates. The energy left behind in a particular vibrational mode will then convert back and forth between potential and kinetic energy with frequency ω_n. At any time, the energy, $U_n(t)$, in a particular mode of vibration is

$$U_n(t) = \tfrac{1}{2} k_n \phi_n^2(t) + \tfrac{1}{2} a_n \dot{\phi}_n^2(t) , \tag{25}$$

where k_n and a_n are the stiffness constant and coefficient of

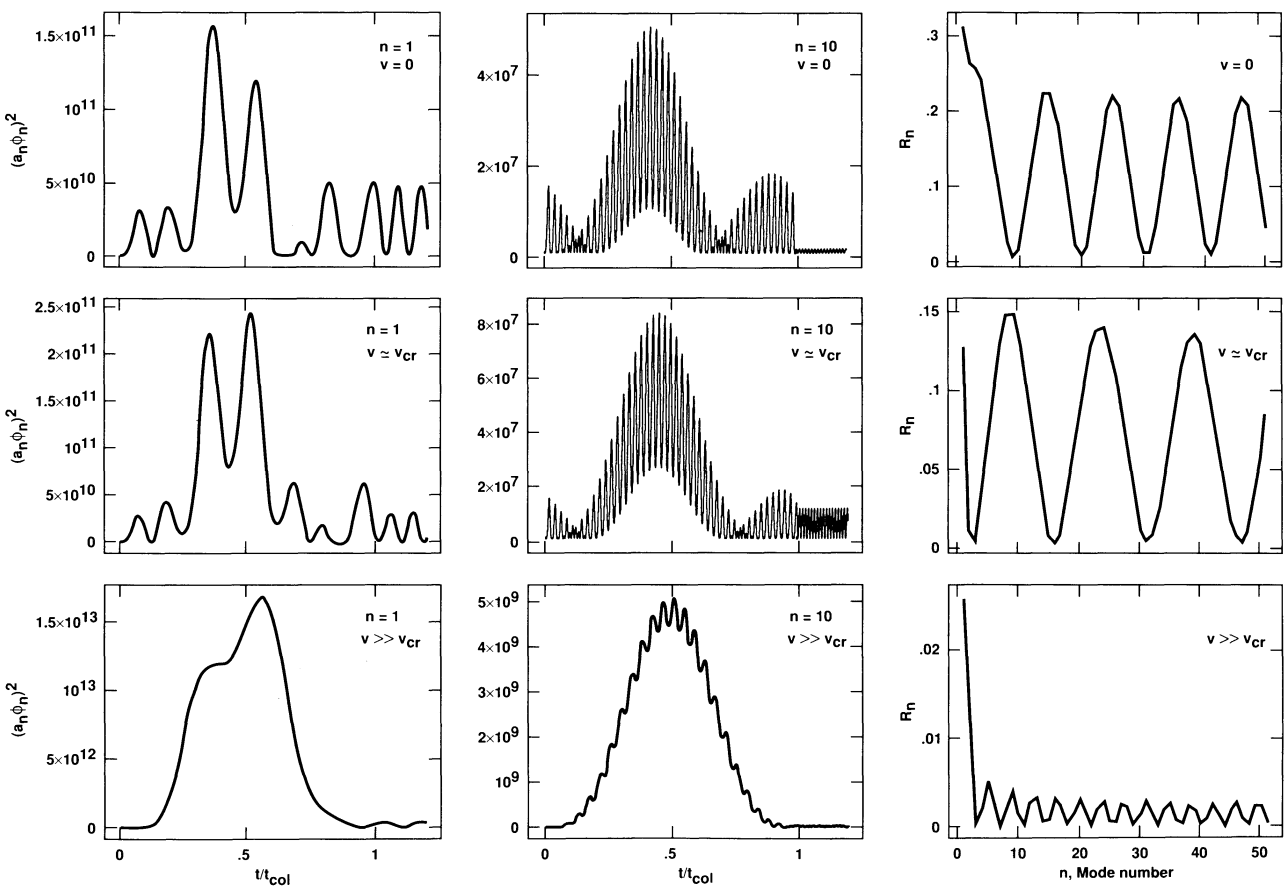

FIG. 6.—Deformation ($[a_n \phi_n]^2$) associated with mode $n = 1$ and $n = 10$ for three different collision velocities: (1) $v = 0$ (*top row*), (2) $v \simeq v_{cr}$, the critical velocity for sticking (*middle row*), and (3) $v \gg v_{cr}$ (*bottom row*). Also shown (*left column*) is the fraction, R_n, of the collision energy left behind in a mode as a function of mode number, n, for these three collision velocities.

inertia, which are related through $\omega_n = \sqrt{k_n/a_n}$. The time evolution of the kinetic energy in a mode, and thus of the potential energy as well, is thus proportional to $\phi_n^2(t)$. The coefficients a_n would have to be evaluated from Lamb's theory for such vibrations (1882). However, that is rather involved, and we have opted for a simpler approach. Recognizing that many modes will be excited, we will instead estimate the average energy left behind in a mode after the collision process and compare that to the total collision energy available before collision. We define R_n as the ratio of the total energy in a mode after collision ($U_n[t > t_{col}]$) to the maximum energy imparted to the same mode during the collision process ($U_n[t = t_{max}]$)

$$R_n = \frac{(a_n \phi_n)^2_{t>t_{col}}}{(a_n \phi_n)^2_{t=t_{max}}} . \quad (26)$$

Here t_{max} is the time at maximum compression, and the $a_n \phi_n$ are the maximum values measured near the indicated times to account for the exchange between kinetic and potential energy of the waves.

R_n is plotted as a function of the mode number for the three collision velocities $v = 0$, $\sim v_{cr}$, $\gg v_{cr}$ in Figure 6. This energy ratio shows a sinusoidal behavior with mode number, n. Essentially, R_n varies as $\sim \sin^2(\omega_n t_{col})$, not entirely surprising given the convolution of a "sinusoidal-like" forcing function with sinusoidal waves. The average energy left behind in the waves after the collision, relative to the maximum elastic energy during collision, can thus readily be determined numerically. The maximum energy in elastic modes at $t = t_{max}$ is equal to $U_{col} + |U_S|$ (see eq. [18]), and this can be related to the kinetic energy at infinity, U_K via equation (17). Figure 7 shows the ratio U_{lost}/U_K as a function of U_K expressed in dimensionless units by ratioing to the interaction energy, $F_c \delta_c$. This figure was constructed from a large number of individual runs for various initial velocities and material parameter combinations. Recalling that the forcing function is written in dimensionless form (eq. [11]), the only place the material parameters enter is in determining the velocity at contact, v_{col}, and in the relative kinetic energy itself, $U_K/F_c \delta_c$. Our normalization choice for Figure 7 completely eliminates these dependences. Indeed, all our numerical results agree very well and give rise to the single relationship shown in Figure 7 despite the large range assumed for γ and E (factor 10^3).

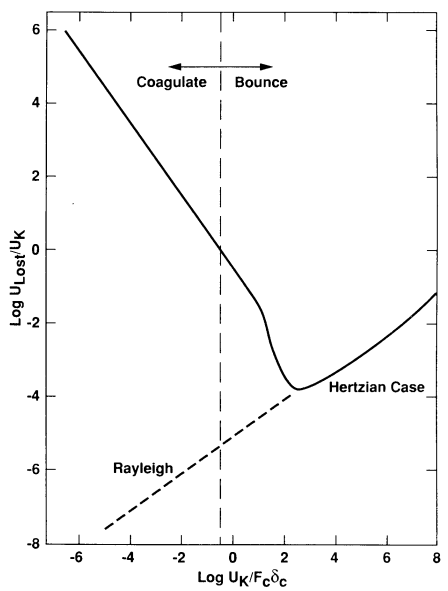

FIG. 7.—Energy left behind in the grains U_{lost} after the collision as a function of the kinetic energy at contact U_K. The factor $F_c \delta_c$ measures the interaction energy of the grains. The normalization employed makes this a universal curve, independent of the absolute collision energy and material parameters. The dashed curve presents the results from Rayleigh's (1906) analysis which ignores the attractive interaction energy. It is shown that for collision energies much larger than the interaction energy ($U_K \gg F_c \delta_c$) our results asymptote to those of Rayleigh.

As Figure 7 demonstrates, the energy lost in a collision is approximately constant (i.e., $U_{lost}/U_K \propto U_K^{-1}$) as long as the kinetic energy is smaller than the attractive potential energy (i.e., $U_K < F_c \delta_c$) and a large number of modes are excited (see below). Specifically, U_{lost} is well represented by

$$U_{lost} = c_1 F_c \delta_c \quad (27)$$

with $c_1 \simeq 0.4$. Thus, as in our quasi-static analysis, we find that the energy lost is proportional to $F_c \delta_c$ and independent of the initial kinetic energy. However, the absolute amount of energy lost in the collision is now much larger than in the quasi-static analysis (e.g., 0.4 vs. 0.09). Clearly, the energy present in elastic waves outside of the contact area is considerably larger than the deformation energy associated with the contact area at tear-off. For high initial kinetic energies, $U_K \gg F_c \delta_c$, the attractive potential (stickiness) has little effect, and the energy lost becomes Hertzian, $U_{lost}/U_K \propto \sqrt{U_K}$ (Rayleigh 1906). Here the particles bounce. Formally, U_{lost}/U_K will exceed unity for high enough U_K in the Hertzian limit, and coagulation would be implied; however, in reality, shattering and vaporization occur long before this limit is reached.

It should be emphasized that, at low temperatures, dissipation of the excited wave energy is a very slow process. Attenuation of sound waves is largely due to their interaction with other phonons (Brüesch 1986). At low temperatures ($T < \Theta_D$ with Θ_D the Debye temperature, i.e., low phonon occupation number), sound wave attenuation is small; at 30 K, attenuation is typically $\simeq 3$ dB cm^{-1} for frequencies $\nu \simeq 10^{10}$ s^{-1} and scales directly with the frequency and with the temperature to the fourth power. This corresponds to a dissipation time scale of $\simeq 10^{-5}$ s, which is much longer than the collision time scale of micron-sized dust grains ($\simeq 10^{-9}$ s; § 2.2.1). At high temperatures ($T > \Theta_D$), the attenuation, α, is given by $\alpha = \gamma^2 \nu^2 T \sigma / \rho C_s^5$ with γ the Grüneisen constant of the material. Now, at high temperatures, the thermal conductivity, σ, is inversely proportional to T. Adopting a $\sigma \times T$ of 6×10^8 ergs cm^{-1} s^{-1} appropriate for ice leads then to dissipation time scales which are still much longer than the collision time. Silicates have somewhat larger $\sigma \times T$ ($\simeq 6 \times 10^9$ ergs cm^{-1} s^{-1}), but still dissipation plays little role. In contrast for metals or semimetals such as graphite in the basal direction, dissipation is very rapid at high temperatures. Thus, at typical interstellar dust temperatures (10–20 K), direct energy dissipation plays no role during the actual collision, but in the inner solar nebula it can have played a role for metallic grains. Finally, it should be emphasized that, even at low temperatures, eventually any collision and binding energy remaining in the colliding grains will be converted into heat on the dissipation time scale and will be radiated away.

2.3. *The Critical Velocity*

For sticking to occur on collision, the energy remaining in elastic waves at $t = t_{col}$ should be greater than the initial

kinetic energy U_K. We define the critical velocity, v_{cr}, as the collision velocity for which the energy lost is exactly equal to the kinetic energy at infinity. It is, thus, the highest velocity for which sticking will occur. Substituting for F_c and δ_c (see § 2.1), we find then

$$v_{cr} \simeq 3.86 \frac{\gamma^{5/6}}{E^{1/3} R^{5/6} \rho^{1/2}} . \quad (28)$$

Thus, a material with a smaller Young's modulus, E, will stick better because it will more readily deform, leading to a larger contact area. Similarly, a larger surface energy, γ, will lead to increased binding across the contact area and therefore to an increased critical velocity. Finally, the critical velocity is a decreasing function of the size of the colliding grains in our model. Essentially, this results from the large surface to volume ratio in small grains and hence the larger ratio of binding to kinetic energy. This is also obvious when comparing the radius of the zero load equilibrium contact circle with the grain size

$$\frac{a_0}{R} = \left(\frac{9\pi\gamma}{RE}\right)^{1/3} . \quad (29)$$

Thus, smaller particles form larger contact areas relative to their size and therefore coagulate better. The enhanced agglomerative properties of smaller particles has been observed and discussed in detail by Kendall (1980).

Figure 8 shows the critical velocities derived for collisions between two equal grains of ice, graphite and quartz, respectively, as a function of particle size. Small particles (~ 100 Å) can collide with initial relative velocities as high as a $\sim 10^4$ cm s^{-1} and still stick. For micron-sized particles critical velocities are of the order of $\sim 10^2$ cm s^{-1}. We also conclude that for equal sizes, icy particles stick better than silicate particles. Two factors contribute to enhanced adhesivity for contacts between ice surfaces. The higher interface energy (Table 3) results in a larger binding energy of two grains. Moreover, the smaller Young's modulus increases the contact area due to increased elastic deformation. The coagulated grains have therefore both increased binding energy per unit surface and increased contact area (see § 2.1).

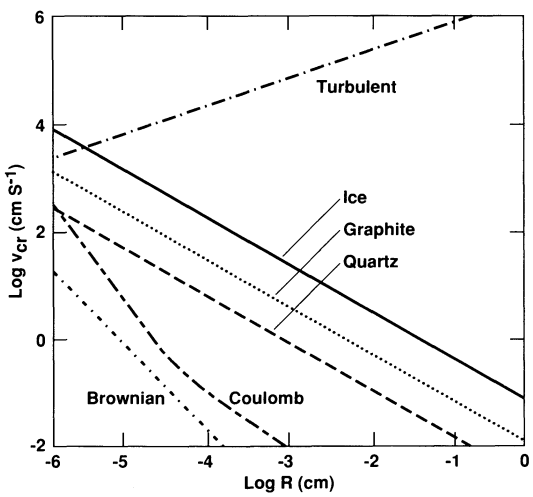

FIG. 8.—Critical velocity, v_{cr}, for sticking as a function of grain size, R, for three materials (quartz, graphite, and ice). For $v < v_{cr}$ two colliding grains will stick, while for $v > v_{cr}$ they will bounce. The curves labeled Brownian and turbulent refer to the expected grain velocities due to random thermal motion and turbulent motion in interstellar clouds, respectively. The curve labeled Coulomb represents the minimum velocity required to overcome the repulsive Coulomb barrier between charged grains (*see text*).

2.4. *Comparison with Rayleigh's Analysis*

Rayleigh (1906) investigated the vibrations excited by colliding spheres and the associated loss of translational energy of the particles. He concluded that for a wide range of collisional velocities, the energy loss to vibrations was very small and did not exceed more than a few percent of the collision energy for relative velocities of the order of the sound speed in solids ($\sim 10^6$ cm s^{-1}). Indeed, his results predict that small (≤ 1 μm) grains colliding at 10^2 s^{-1} would lose only 10^{-5} of their kinetic energy on collision. In contrast, in our calculations, such grains lose all their translational kinetic energy to wave excitations and coagulate. Two important differences are responsible for the very disparate results in the two cases. First, Rayleigh assumed that in a collision process most of the energy would be carried by the longest period mode available, that is, the $n = 1$ mode. Thus, to determine the energy loss in a collision he compared the energy retained by this mode after the collision to the kinetic energy of collision. We find that a substantial fraction of energy is lost to higher frequency modes. Essentially, for our collision parameters, $\omega_n t_{col} \gg 1$ for $n \simeq \tilde{n}$, and many modes will couple equally well to the forcing function. Second, Rayleigh's calculations ignored the attractive interaction across the contact area. This interaction leads to larger contact areas and larger collision velocities, resulting in enhanced translational energy loss between particles colliding at (initially) low relative velocities.

It should be emphasized that Rayleigh's analysis becomes important in the limit of high initial velocities when the initial kinetic energy is much larger than the binding energy. The bottom panels in Figure 6 shows the wave excitations and fractional energy lost for such collisions (i.e., $v \gg v_{cr}$). In contrast to low-velocity collisions, the energy is now mainly lost to the lowest modes, essentially because in this case $\omega_n t_{col} \simeq 1$ and these modes couple much better to the forcing function. Rayleigh's relation for energy loss in colliding graphite particles is compared to our numerical results in Figure 7. We also show U_{loss} calculated from our numerical analyses including only the lowest frequency mode. We find that, when $U_K \gg F_c \delta_c$, the energy lost to the first mode agrees reasonably well with Rayleigh's result.

2.5. *Comparison with Experimental Studies*

Dahneke (1975) has studied the energy lost by micron-sized polystyrene grains bouncing on a quartz substrate. This study shows that at high incident velocities, $v_i > 200$ cm s^{-1}, the velocity measured after the bounce, v_r, is constant at about $0.96 v_i$. However, v_r/v_i drops rapidly to zero for v_i less than about 200 cm s^{-1} (Fig. 9).

Our model can be applied to this case—a sphere bouncing off a flat surface—as well by substituting for the "reduced" radius the radius of the sphere. The rebounding velocity can then be determined from the final energy, $U_f = U_K - U_{lost}$, using $v_r = \sqrt{2U_f/m}$. Varying the free parameters, γ and E, within reasonable bounds, we find that the solution is most sensitive to the value adopted for γ. Our model provides a good fit to the data for $\gamma = 340$ ergs cm^{-2}. Estimates for the material parameters of polystyrene and quartz are provided in Table 3. The Young's modulus measurements refer to bulk materials. The interface energies have been directly determined

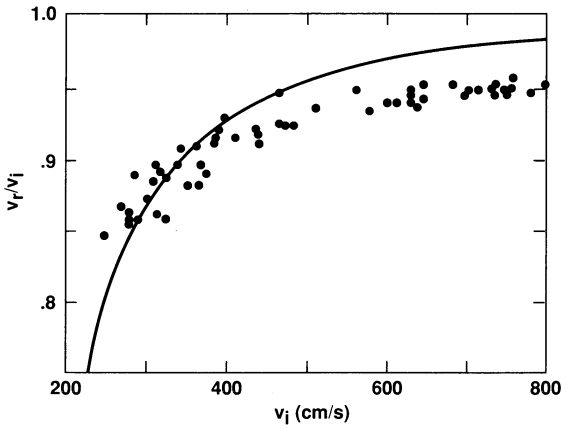

FIG. 9.—Velocity upon reflection, v_r, as a function of the incident velocity, v_i. Dots are the data measured for micron-sized polystyrene spheres bouncing on a quartz slab. The line presents our best fit to this data.

from experimental measurements of contact area of micron-sized polystyrene and silicate particles under zero external force (Kendall & Padget 1987; Kendall et al. 1987). The surface energy inferred from Dahneke's bouncing experiments (340 ergs cm^{-2}) is much higher than expected for these materials ($\simeq 17$ ergs cm^{-2}; see Table 3). Since the surface energies listed in Table 3 have been measured directly from sticking experiments on small grains, this difference is not understood within the framework of our model. Possibly, plastic work is important (Dahneke 1975). However, that would imply that the plastic yield strength of the material is $\simeq 10^9$ dyn cm^{-2} which is about a factor 5 less than we would estimate (see § 3.4). Moreover, once the velocity exceeds the minimum velocity to start the yielding process, the (excess) kinetic energy would go into more plastic work being done (much like silly putty thrown on the floor faster and faster, deforms more and more). Thus, the rebound velocity shouldn't increase with increasing initial velocity in the plastic regime.

For high impact velocities ($v \geq 500$ cm s^{-1}) the experimental data seem to plateau at about 0.96, while the theoretical curve asymptotes to unity. In the limit of large collision velocity the fraction, f_i, of the incident initial kinetic energy, which remains in the particles as internal excitation energy, can be theoretically evaluated to be (Rayleigh 1906)

$$f_i = 0.02 \frac{v_i}{c_s},$$

where c_s is the velocity of sound in the material (Rayleigh 1906). For polystyrene spheres ($c_s = 1840$ cm s^{-1}) it is expected that f_i is about 10^{-4} for $v_i \simeq 10$ m s^{-1}. Dahneke (1975) suggested that a small amount of plastic work may have caused this discrepancy. However, that seems unlikely (see § 3.4). Some plastic work can be done even below their yield point (elastic hysteresis), but that seems to be more limited than indicated by these experiments ($\simeq 0.4\%$; Johnson 1989).

3. ADHESION OF "REALISTIC" GRAINS

In our derivations we have made several approximations which may not be entirely correct for interstellar dust grains. In particular, our theoretical grains consist of smooth spherical grains, while in reality interstellar grains may be elongated, covered by ice mantles, and have rough surfaces. Moreover, we have neglected plastic deformation, which might be an important additional energy loss channel. Finally, if coagulation is truly important in interstellar space, interstellar grains will consist of fluffy conglomorates of small spheres (see Tielens 1989, 1990b). Crushing and slippage may play an important role in collisions involving such conglomorates. We will discuss each of these effects in this section.

3.1. *Elongated Grains*

Contact deformation of spheroidal grains is slightly more complicated than for spherical grains, but the essence remains. The contact area is now an ellipsoid with axial ratio $(R_a/R_b)^{1/2}$ where R_a and R_b are the principal radii of curvature at the point of contact. The equations governing contact can now be written in the same way as before by replacing the radius of curvature by an equivalent relative curvature $R_e = (R_a R_b)^{1/2}$, except for a small correction factor (Johnson 1989). This correction factor departs rather slowly from unity with increasing ellipticity. For example, the correction to the force-displacement relation—the basis of most of our discussion—is less than 2% when the ratio of the miner to major axis is larger than 0.25. Thus, it is safe to ignore this complication.

3.2. *Core-Mantle Grains*

The waves involved in the deformation of two colliding bodies are so-called Rayleigh waves (Rayleigh 1887; Love 1944). These waves are essentially surface waves with a penetration depth of about one wavelength. It stands to reason then that, as long as the depth of penetration is less than the mantle thickness (i.e., $n \gg 1$; see § 2.2.2), the core-mantle nature of grains has little influence on the collision process. In that case, Young's modulus is given by that of the mantle material. The van der Waals interaction between core-mantle grains will also differ from that of homogeneous bodies. However, since the interaction of H_2O ice mantles will be dominated by hydrogen bonding, this has actually little consequence, and the surface energy of H_2O ice should be used in the analysis. Obviously, since the specific density of the core and mantle material may be quite different, the kinetic energy–grain size relation used in deriving the scaling factor for the critical velocity has to be adjusted accordingly.

3.3. *Surface Roughness*

Interstellar grains could have rather irregular surfaces. In particular, high-velocity impacts of small grains in interstellar shocks will lead to crater formation on size scales comparable to that of the impactor ($\simeq 50$ Å). Likewise, sputtering by impacting gas ions may lead to surface structure on $\simeq 10$ Å scale (Jones et al. 1992). These effects will be counteracted to some extent by the growth of ice mantles inside dense clouds, since binding will be stronger near such surface structures. Transmission electron microscope images of interstellar grains recovered from meteorites show both very weathered and very smooth grains (Tang et al. 1989). It is therefore appropriate to consider the effects of surface structure on adhesion of grains.

Surface roughness is known to have a profound impact on adhesion properties of macroscopic bodies (Fuller & Tabor 1975; Tabor 1977; Johnson 1976). For rough surfaces, real adhesive contact will only occur at the crests of asperities, and consequently the adhesive forces will be reduced compared to the interaction of smooth spheres. Consider a surface with a large number of spherical asperities, each with a radius of curvature R_a. Now, in our case, we have to realize that the radius of the contact area is only somewhat larger than the van der

Waals radius (20–100 Å vs. 4 Å; Table 2), and, compared to macroscopic bodies, this will tend to limit the effect of surface roughness. In our case, we can envision two extremes depending on the size of the asperities with respect to the contact area. For graphitic and silicate grains with their extremely small contact areas (Table 2), it is expected that asperities on their surfaces will be comparable to or larger than the contact area. Ice, in contrast, could be in either limit.

When the asperity is of the order of the size of the contact area or larger, contact will be made with one asperity only. The equations governing contact are the same as before except that the radius of curvature is now equal to R_a rather than R. It is then straightforward to show that the critical velocity for sticking scales with $(2R_a/R_0)^{2/3}$, with R_0 the radius of the (equal) colliding grains. Thus, for 1000 Å ice grains with a surface asperity of 100 Å (the size of the contact area), this reduction in the critical sticking velocity amounts to a factor $\simeq 3$. For silicate and graphite grains this reduction in the critical velocity can be somewhat larger, basically because the contact area for these materials will be smaller.

When the asperities are much less than the size of the contact area, contact will be made with many. Now assume a random distribution of the heights of the asperities above the nominal surface with standard deviation σ. Typically, σ is much less than R_a. Detailed theoretical and experimental studies show that the extent of the reduction in the adhesive forces depends on σ/δ_a where δ_a is the critical displacement δ_c evaluated for the asperity; $\delta_a \simeq 2\sqrt{R_a/10}$ Å for ice. Thus, assuming $R_a = 10$ Å and σ is 50% of the van der Waals interaction radius, $\sigma/\delta_a = 1$ and the pull-off force, F_c is reduced by a factor $\simeq 2$ relative to the smooth sphere case (Fuller & Tabor 1975; Johnson 1976). The characteristic energy involved is now $F_c \times \delta_a$ which is reduced by a factor 5 compared to the collision of smooth (1000 Å) spheres. Thus, the critical velocity will be reduced by a factor $\simeq 2$ from the smooth grain case.

For macroscopic grains ($R \gg 100$ μm), a more detailed theory, has to be developed taking into account the variation of the pull-off force with σ (see Fuller & Tabor 1975), but that is beyond the scope of this paper.

3.4. *Plastic Deformation*

For macroscopic bodies, plastic deformation can be an important energy sink in low-velocity impacts. However, this is less so for micron-sized particles. Largely independent of the details of the yield criterion (i.e., von Mises or Tresca; Johnson 1989), onset of yielding will occur when the maximum contact pressure, p_y, reaches the critical value of $\simeq 1.6\ Y$, with Y the yield strength of the material in simple tension. The force required for yielding is then given by

$$F_y = \frac{\pi^3 R^2}{6E^2} p_y^3 \simeq 21 \frac{R^2 Y^3}{E^2} . \tag{30}$$

For a perfectly elastic-plastic material, the displaced material will be accommodated by an elastic compression of the surrounding solid. We can compare this yielding force to the forces experienced during collision,

$$\frac{F_y}{F_c} = 7.6R\left(\frac{Y}{E}\right)^2 \frac{Y}{\gamma} . \tag{31}$$

When $F_y/F_c < 1$, the collision will result in plastic flow which will enhance coagulation. Now, for macroscopic metal[1] bodies, plastic flow occurs by slip—the motion through the lattice of a dislocation (Kittel 1976)—and as a result the yield strength, Y, is generally orders of magnitude less than Young's modulus. However, typically, the density of dislocations, the number of dislocations that intersect a unit plane, is $\simeq 10^8$ cm^{-2}. Thus, a submicron-sized grain will be intersected by only a few dislocations (fluffy aggregates will be discussed in § 3.5). Moreover, the forces required to activate a dislocation are inversely proportional to its length, and hence small size scales will be less prone to yielding. Consequently, the yield strength of a particle is expected to approach the ultimate yield strength of the material. In that case, Y/E will be about 0.2, largely independent of material (Petch 1968). We can then write for equation (31)

$$\frac{F_y}{F_c} \simeq 60\left(\frac{R}{1000\ \text{Å}}\right)\left(\frac{E/\gamma}{10^8\ \text{cm}^{-1}}\right) . \tag{32}$$

Typical values for E/γ range from 2×10^8 to 3×10^9 cm^{-1} (see Table 3). Now for impact velocities less than the critical velocity, F/F_c is less than about 3 (see Fig. 3). Hence, plastic deformation can be important in ice grain collisions for sizes less than 50 Å. For graphite, quartz, and iron grains this maximum size for which plastic deformation is important is even smaller.

Turning this point around, we can use equation (30) to estimate the critical impact velocity required to start plastic deformation for a given grain size. Since we are well above the critical velocity for adhesion, we may use equations (1)–(4) to yield

$$\frac{1}{2}\mu v_{\text{pd}}^2 \simeq 54 \frac{R^3 Y^5}{E^4} . \tag{33}$$

For like grains, and using $C_s^2 = E_1/\rho$, this translates into $v_{\text{pd}} = 0.032C_s$, or typically, 10^4 cm s^{-1}. In contrast, for a macroscopic (centimeter-sized) steel ball with $Y \simeq 10^{10}$ dyn cm^{-2} ($\simeq 10^{-2}E$), this velocity is only 10 cm s^{-1}. Now, at this impact velocity, the plastic zone is confined to a small region right below the impact point. When the impact force increases, this plastic zone expands until it breaks out to the surface. At that point, the plastic material will flow to the sides, and a crater will be created. The contact pressure required for uncontained plastic flow is only somewhat larger than that required for the onset of yielding; that is, $p_f \simeq 3Y$ (Johnson 1989). For micron-sized particles, this corresponds to an impact velocity of $v \simeq 0.15C_s$ or typically 0.4 km s^{-1}. This is in good agreement with laboratory studies on crater formation by impacting micron-sized grains (Neukum et al. 1970; Bloch et al. 1971; Mandeville & Vedder 1971; Vedder & Mandeville 1974). The carved-out material will then flow along the crater walls and form a crater lip. During this process, a large fraction of the plastically flowing material will be ejected in the form of small fragments, and much of the initial collision energy will go into the formation of these fragments and their kinetic energy. The majority of these collisions will lead to mass loss rather than grain growth. This will be discussed in an astrophysical context by Jones et al. (1992).

In summary, plastic deformation is an important energy sink in the collision of macroscopic metal spheres, even at low impact speeds (10 cm s^{-1}). For micron-sized spheres, plastic

[1] Macroscopic brittle bodies such as ceramics will shatter rather than plastically deform.

deformation does not start until impact velocities of $\simeq 10^4$ cm s^{-1}. For somewhat larger impact velocities ($\simeq 5 \times 10^4$ cm s^{-1}), a crater will form, and a large fraction of the crater volume will be ejected in the form of small fragments. In the intermediate velocity range, plastic welding may lead to enhanced adhesion properties compared to the elastic theory developed in this paper.

3.5. *Fluffy Grains*

Two effects have to be considered in the collision of fluffy agglomorates. First, adhesion will be governed by the local properties of the collision partners, but the kinetic energy by the whole system. As for asperities—indeed this is one way large asperities could be created—the local radius of curvature will enter into the critical sticking velocity. For example, assuming only a single contact point in the collision of two conglomorates consisting of N equal "monomer" grains of radius R, the critical velocity will scale with $N^{-1/2} \times R^{-5/6}$ and decreases fast with increasing number. For more than one contact point, this relation will change somewhat, but the essential point, decreasing critical velocity with increasing number, is still correct. Addition of a single monomer to an existing conglomorate will have a critical velocity quite comparable to that of two colliding monomers, since both the local radius of curvature and the reduced mass (i.e., the kinetic energy in the center of mass frame) will be quite similar. In contrast, large conglomorates stick inefficiently (the critical velocity decreases by a factor $N^{-1/2}$) compared to their "monomers." Thus, the collisional growth of an agglomorate will typically be dominated by addition of the smallest units available. Of course, the collision of two fluffy conglomorates will have a higher critical velocity than the collision of two homogeneous grains with the same size due to much reduced mass of the former as compared to the latter.

The second effect to be considered is that the collision may lead to slippage at the individual grain boundaries of the monomers making up the conglomorates. Depending on the geometry of the agglomorates, this may either lead to the formation of more than one contact area and hence increase adhesion, or it may actually lead to the fragmentation of the conglomorate into a number of smaller pieces. The crushing involved in the former process might be particularly effective in compact agglomorate structures, while shattering may dominate for open structures. Clearly, estimating the critical velocity of agglomorates is a sticky business since it not only involves the detailed microphysics of the adhesion process but also the geometry of the collision and the retained memory of the collisional growth process. Nevertheless, further studies are well warranted if one wants to understand the coagulation of solid agglomorates.

4. ASTROPHYSICAL IMPLICATIONS

4.1. *Grain Charge*

In coagulating environments in the interstellar medium, such as dense molecular clouds or protoplanetary disks, grains are likely to have an equilibrium charge. The presence of charges on the grain may influence the collisional behavior of grains. We briefly investigate this aspect here. This charge results from the balance between adsorption of electrons and ions from the gas. This gas is ionized by cosmic rays and by the decay of radioactive elements (i.e., ^{40}K). The higher thermal speed of the electrons compared with the ions results in a higher flux of electrons than ions and consequently in excess negative charge on the grain (see Spitzer 1978). Equilibrium is achieved when the grain surface electric potential is of order $-2.5kT_g$, corresponding to a grain charge $q = 2.5kT_g R/e$ with R the grain radius and T_g the gas temperature (20 K adopted hereafter). For small grains, this yields a fractional unit charge; that is, the grain will only carry a charge part of the time. In our analysis we adopt the unit charge. Larger grains carry the calculated charge rounded to the nearest integer.

The potential $\phi(\rho)$ between two equal spheres of radii R, separated by a distance ρ and carrying charges $q_1 = q$ and $q_2 = sq$ at their centers, respectively, can be written as (Fuchs 1964)

$$\phi\left(\frac{2R}{x}\right) = \frac{q^2}{2R} \times \left[s\left(x + \frac{15}{448}x^7 + \cdots\right) - (1 + s^2)\left(\frac{x^4}{16} + \frac{x^6}{64} + \cdots\right)\right], \quad (34)$$

where $x = 2R/\rho$. We define D as the distance between the closest surfaces of the two spheres (i.e., $\rho = 2R + D = 2R/x$ and $x = 2R/[2R + D]$). Thus, when the two spheres touch and D goes to zero, x goes to one. The first term in the series is the potential between point charges. The rest of the terms represent induction and are derived using the method of image charges. Note that even near contact, the potential between two equal spheres always remains repulsive, and thus a minimum kinetic energy is required to overcome the potential barrier. For two equal grains, we calculate the minimum velocity, $v_{\min}$, needed to overcome the Coulomb barrier at contact which is defined as $D = 4$ Å. This minimum velocity is plotted in Figure 8. The required minimum kinetic energy scales with q^2/R which is proportional to R for equal spheres. Thus, the minimum velocity scales with R^{-1}, as evident in Figure 8 for large grain sizes. Small grains essentially carry excess charge (i.e., unit charge) compared to their expected equilibrium value, and the dependence of $v_{\min}$ on grain size steepens. This steepening occurs around 500 Å for our parameters (Fig. 8). Therefore for small grains to coagulate, they must have velocities above this minimum velocity, but less than the critical velocity for sticking. As Figure 8 demonstrates, over most of our parameter space the minimum Coulomb velocity is less than the critical sticking velocity, and coagulation is physically possible. Moreover, the smallest grains will be neutral part of the time and thus the Coulomb interaction with a charged grain will be attractive rather than repulsive through the formation of an image charge (see eq. [30]).

4.2. *Turbulent and Brownian Motions of Particles*

Coagulation of dust grains in astrophysical environments can be driven by either Brownian or turbulent motions. For Brownian motions, we adapt the expression given by Draine (1985) for Brownian velocities in dense molecular clouds as a function of particle size ($v \simeq 3$ (1000 Å/R)$^{1.5}$ cm s^{-1}). As expected, grain velocities due to Brownian motions are very small and below the critical velocity for sticking for all the materials considered (Fig. 8). Thus, all Brownian collisions will lead to coagulation. However, the time scales involved are exceedingly long, and coagulation driven by Brownian motions is completely negligible in dark clouds (see Tielens 1989).

The coagulation rate can be enhanced by the presence of

turbulence, which enhances the relative grain velocities. Volk et al. (1980) and Draine (1985) have analyzed relative grain velocities in turbulent clouds with a Kolmogorov spectrum of turbulent eddies. Grains larger than a critical size (Weidenschilling 1984; Markiewics, Mizuno, & Volk 1991) will couple efficiently to macroscopic turbulence, typically to those eddies with size scales comparable to their stopping length. Since the stopping length will depend on the mass of the grain, different-sized grains will acquire substantial relative motions. The gas flow on the smallest scales will, however, be laminar, and thus grains with stopping lengths comparable to these small scales do not couple to the turbulence. At densities of 10^3–10^5 cm^{-3}, this critical grain size ranges from 100–250 Å. Smaller grains than this will thus exhibit a Brownian (thermal) velocity spectrum, and collisions among them are unimportant. However, they will still collide with large grains at the turbulent velocities of the latter and may still be swept up efficiently. Relative grain velocities of about 70 m s^{-1} are expected for 1000 Å grains at a density of 10^4 cm^{-3} in molecular clouds, and this velocity increases with grain size (Fig. 8). Thus, silicate or graphite grains will not coagulate at this density. The turbulent velocity will decrease with increasing density, but densities in excess of 3×10^5 cm^{-3} are required to drop the turbulent velocity below the critical sticking velocity for a 1000 Å graphite grain. The formation of an accreted ice mantle on such grains can, however, increase the critical velocity for sticking considerably, and, in general, this will promote coagulation (Tielens 1989). This conclusion is based upon sticking coefficients evaluated for smooth grain surfaces. The presence of surface irregularities will decrease the critical velocity by perhaps a factor 3 for ice and much larger for silicate and graphitic grains. Consequently, this suggests that, even for ice-covered grains, densities well in excess of 10^4 cm^{-3} are required for coagulation to occur.

In order to determine the importance of coagulation, the coagulation time scale has to be compared to the evolutionary time scale of the molecular cloud. For densities $\leq 10^4$ cm^{-3}, molecular clouds are probably supported by magnetic fields and turbulence and live much longer than their free fall time scales; perhaps as long as 10^8 yr. However, as discussed above, the turbulent velocities of the grains may prevent coagulation during this phase of molecular cloud evolution. Eventually, dense cores may form via ambipolar diffusion, and the gas may begin to collapse under the influence of its own self-gravity. At densities in excess of 10^4 cm^{-3}, the free-fall time scale ($\tau_{ff} = 10^8/n^{1/2}$ yr) is probably a reasonable estimate of the evolutionary timescale. Limiting ourselves to "classical" grains (i.e., with $a > 1000$ Å and total grain surface area of 5×10^{-22} cm^2/H – atom) which contain the bulk of the grain mass, the coagulation time scale is independent of the density ($\tau_c \simeq 3 \times 10^6$ yr) because the collision velocity due to turbulence scales inversely with the density. For densities in excess of 10^4 cm^{-3} (i.e., velocities below the critical sticking velocity), the ratio of the coagulation time scale to the free-fall time scale is then

$$\tau_c/\tau_{ff} = 3 \times 10^{-2}\sqrt{n}\,, \qquad (35)$$

and coagulation never dominates, once a cloud begins free-fall contraction.

Thus, in conclusion, coagulation in interstellar clouds requires icy grain mantles (i.e., high critical velocity for sticking) and densities well in excess of 10^4 cm^{-3} (i.e., dense star-forming cores). Even then, coagulation is only of limited importance, resulting in perhaps a doubling of a grain's mass within a dynamical evolution time scale (see eq. [31]). However, because of their higher critical sticking velocities, small grains ($a \ll 1000$ Å) will be efficiently swept up by large grains, and thus are removed from the grain size distribution, even at densities of 10^4 cm^{-3} (Fig. 8). As a result, the interstellar extinction curve in dense cores will be quite different from that in the diffuse interstellar medium, particularly in the ultraviolet (i.e., weakening of the 2200 Å bump and the far-UV rise). Since the near- and mid-infrared emission from the interstellar medium is dominated by temperature fluctuations in small grains ($a \leq 50$ Å), the removal of the smallest grains sizes will also have a profound influence on the emitted IR spectrum.

5. SUMMARY AND CONCLUSIONS

We have theoretically modeled the collision of two small spherical particles, using elastic continuum theory for the description of the solids. Two bouncing grains come into contact, form a contact area which grows as the grains continue to drive into each other, stop, repel each other as their compressed shapes spring back to normal, pull out an elongated neck as their adhered surfaces "refuse to let go," and finally tear apart at the neck. Two coagulating grains initially behave similarly, except they lack the energy to stretch the neck to the breaking point. Energy has been lost to elastic waves (vibrations) as well as to the deformation energy required to produce the neck. We find that the former dominates by a factor 4–6. The energy lost in the coagulating collision is of the order of the interaction energy required to separate the two coagulated grains when they are at rest and in equilibrium.

We contrast our results to the work of Rayleigh (1906), who ignored the attractive interaction between the particles. We show that our results asymptote to his results in the limit of large collision energies ($\gg$ attractive potential), where the particles bounce.

The collision of two small dust particles will lead to coagulation of the particles for collision speeds less than a critical velocity, $v_{cr} \sim 10^3(100\ \text{Å}/R)^{5/6}$ cm s^{-1}, where R is the reduced radius of the particles. The critical speed is also dependent on the Young's modulus E, surface binding energy γ, and density of the grain material as shown in equation (28). Materials with smaller E have larger v_{cr} (coagulate more readily) because they more readily deform in the collision and transform collision energy to internal vibrations. Materials with higher γ have larger v_{cr} because their stronger attractive forces accelerate the colliding particles, producing more deformation and internal vibrations in the collision.

We have examined the effects of several approximations in our analysis. Of particular importance is the presence of surface structure which will reduce the critical sticking velocity by a factor $\simeq 3$ for ice grains and much more for silicate and graphite grains. Plastic work is an important energy loss channel for centimeter-sized metal spheres. However, micron-sized grains have a much enhanced yield strength, and plastic deformation is of little importance. Finally, we have briefly examined sticking of fluffy grain agglomorates. In this case, sticking will not only depend on the microphysics of the adhesion process but also on the geometry of the collision and the collisional history of the agglomorates (i.e., open vs. compact structures). Likely, agglomoration will occur primarily through the addition of "monomers" rather than "N-mers."

Further work on the growth process of such structures will be very valuable.

We have briefly applied our basic results to interstellar conditions. We find that the effect of grain charge is negligible, except at very low ($v \ll v_{cr}$) collision speeds where the Coulomb repulsion prevents the grains from ever touching. Brownian motion of neutral grains in interstellar clouds would lead to coagulation ($v \ll v_{cr}$), but the Brownian speeds are so small that the coagulation rate is negligible. Relative grain motion is dominated by turbulent fields, and we have applied a model for the turbulent grain velocities developed by Volk et al. (1980) and Draine (1985). Small grains ($< 10^2$ Å) do not couple efficiently to the turbulent velocity field. However, classical 0.1 μm dust grains will acquire high relative velocities ($v > v_{cr}$) in the bulk of molecular clouds where the gas density is less than 10^4 cm^{-3}, and these grains will bounce upon collision. In dense molecular cores ($n \gg 10^4$ cm^{-3}), large grains have speeds $v \leq v_{cr}$, and coagulation proceeds. However, such dense cores are often in free fall, and the ratio of the coagulation time to the free-fall time is shown to increase with increasing gas density. Even in this dense gas, therefore, coagulation is only of limited importance, possibly only doubling the grain's characteristic mass within a dynamical evolution time scale. Nevertheless, coagulation will remove small grains ($a \ll 1000$ Å) and PAHs efficiently from the grain size distribution in molecular clouds, resulting in dramatic changes in the interstellar extinction curve and in the near-infrared emission spectrum of the dust.

We are indebted to S. Iijima for permission to reproduce Figure 1. We thank Jeff Cuzzi and Stu Weidenschilling for helpful discussions and their stimulating interest in this subject. Theoretical studies of interstellar dust at NASA Ames is supported under task 399-20-01-30 through NASA's Theory Program.

REFERENCES

Andrews, J. P. 1930, Phil. Mag. Series 7, 9, 593
Bloch, M. R., Fechtig, H., Gentver, W., Neukum, G., & Schneider, E. 1971, Proc. 2d Lunar Sci. Conf., 3, 2639
Bradley, J. P., Sandford, S. A., & Walker, R. M. 1988, in Meteorites and the Early Solar System, ed. J. F. Kerridge & M. Mathews (Tucson: Univ. Arizona Press), 861
Brocklehurst, J. E. 1977, Phys. Chem. Carbon, 13, 145
Brownlee, D. 1987, in Interstellar Process, ed. D. Hollenbach & H. Thronson (Dordrecht: Reidel), 513
Brüesch, P. 1986, Phonons: Theory and Experiments II (Berlin: Springer)
Dahneke, B. 1972, J. Colloid Interface Sci., 40, 1
———. 1975, J. Colloid Interface Sci., 51, 58
Derjaguin, B. V., Muller, V. M., & Toporov, Yu. P. 1975, J. Colloid Interface Sci., 53, 314
Draine, B. T. 1985, in Protostars and Planets II, ed. D. C. Black & M. S. Matthews (Tucson: Univ. Arizona Press)
Easterling, K. E., & Thölen, A. R. 1972, Acta Met., 20, 1001
Fuchs, N. A. 1964, The Mechanics of Aerosols (Oxford: Pergamon)
Fuller, K. N. G., & Tabor, D. 1975, Proc. R. Soc. Lond. A., 345, 327
Gafney, C. 1985, in Ices in the Solar System, ed. J. Klinger (Dordrecht: Reidel), 119
Hertz, H. 1896, Miscellaneous Papers (New York: Macmillan), 146
Iijima, S. 1987, Japanese J. Appl. Phys., 26, 365
Israelachvili, J. N., & Tabor, D. 1973, in Progress in Surface and Membrane Science, ed. J. F. Danielli, M. D. Rosenberg, & D. A. Cadenhead (New York: Academic), 1
Johnson, K. L. 1976, in Theoretical and Applied Mechanics, ed. W. T. Koiter (Amsterdam: North Holland), 133
———. 1989, Contact Mechanics (Cambridge: Cambridge Univ. Press)
Johnson, K. L., Kendall, K., & Roberts, A. D. 1971, Proc. R. Soc. Lond. A., 324, 301
Jones, A. P., Tielens, A. G. G. M., Hollenbach, D., & McKee, C. F. 1992, in preparation
Kendall, K. 1980, Contemp. Phys., 21, 277
Kendall, K., & Padget, J. C. 1987, J. Adhesion, 22, 39
Kendall, K., Alford, N. M., & Birchall, J. D. 1987, Nature, 325, 794
Kittel, C. 1976, Solid State Physics (New York: Wiley)
Lamb, H. 1882, Proc. Lond. Math. Soc., 13, 189
Landau, L. D., & Lifshitz, E. M. 1959, Theory of Elasticity (Oxford: Pergamon)
Love, A. E. H. 1944, A Treatise on the Mathematical Theory of Elasticity (London: Dover)
Mandeville, J.-C., & Vedder, J. F. 1971, Earth Plan. Sci. Lett., 11, 297
———. 1974, J. Geophys. Res., 79, 3247
Markiewics, W. J., Mizuno, H., & Volk, H. J. 1991, A&A, 242, 286
Mathis, J. S. 1990, ARA&A, 28, 37
Mathis, J. S., Rumpl, W., & Nordsieck, K. H. 1977, ApJ, 217, 425
Merrill, K. M. 1977, in The Interaction of Variable Stars with their Environment, ed. R. Kippenhahn, J. Rahe, & W. Strohmeier (Veroff. Remis Stren. Bamberg), Bd. 11, 121, 446
Muller, V. M., Yushchenko, V. S., & Derjaguin, B. V. 1980, J. Colloid Interface Sci., 77, 91
———. 1983, J. Colloid Interface Sci., 92, 92
Neukum, G., Mehl, A., Fechtig, H., & Zahringer, J. 1970, Earth Plan. Sci. Lett., 8, 31
Petch, N. J. 1968, in Fracture I, ed. H. Liebowitz (New York: Academic), 351
Physics Vademecum. 1981, ed. H. L. Anderson (New York: AIP)
Rayleigh, J. W. S. 1887, Lond. Math. Soc. Proc., 17, 4
———. 1906, Phil. Mag., 11, 283
Scalo, J. M. 1977, A&A, 55, 253
Spitzer, L. 1978, Physical Processes in the Interstellar Medium (New York: Wiley)
Tabor, D. 1977, J. Colloid Interface Sci., 58, 2
Tang, M., Anders, E., Hoppe, P., & Zinner, E. 1989, Nature, 339, 351
Thölen, A. R. 1980, Phys. Status Solidi B, 60, 153
Tielens, A. G. G. M. 1989, in Interstellar Dust, ed. L. J. Allamandola & A. G. G. M. Tielens (Dordrecht: Kluwer), 239
———. 1990a, in Submillimeter Astronomy, ed. G. D. Watt & A. S. Webster (Dordrecht: Kluwer), 13
———. 1990b, in Carbon in the Galaxy, ed. J. C. Tarter, S. Chang, & D. DeFrees (NASA CP-3061), 59
Tielens, A. G. G. M., & Allamandola, L. J. 1987, in Interstellar Processes, ed. D. Hollenbach & H. Thronson (Dordrecht: Reidel), 397
Van Vlack, L. H. 1965, Met. Eng. Q., 5, 7
Vedder, J. F., & Mandeville, J.-C. 1974, J. Geophys. Res., 79, 3247
Volk, H. J., Jones, F. C., Morfill, G. E., & Roser, S. 1980, A&A, 85, 316
Weidenschilling, S. J. 1980, Icarus, 44, 172
———. 1984, Icarus, 60, 553
Weidenschilling, S. J., & Cuzzi, J. N. 1993, in Protostars and Planets III, ed. E. Levy, J. Lunine, & M. Mathews (Tucson: Univ. Arizona Press), in press
Wesson, P. S. 1973, Ap&SS, 23, 227
Whittet, D. C. B., & van Breda, I. G. 1978, A&A, 66, 57
Wood, J. A. 1987, Workshop on Origin of Solar Systems, ed. J. A. Nuth & P. Sylvester (LPI Technical Report 88-04), 39
Wright, E. L. 1987, ApJ, 320, 818
Zebel, G. 1966, in Aerosol Science, ed. C. N. Davis (London: Academic), 31
Zisman, W. A. 1963, Ind. Eng. Chem., 55, 19